Chapter

Pulse-Current Electrodeposition of Gold

Chun-Yi Chen, Masaharu Yoshiba, Haochun Tang, Tso-Fu Mark Chang, Takashi Nagoshi, Daisuke Yamane, Toshifumi Konishi and Katsuyuki Machida

Abstract

Pulse-current electrodeposition and a sulfite-based electrolyte were used in fabrication of pure gold films. Surface of the pulse-electrodeposited gold film possessed less defect, lower roughness, smaller grain size, and denser texture when compared with the gold film prepared by constant-current electrodeposition. Microstructures and compressive yield strength of the electrodeposited gold could be controlled by regulating the pulse on-time and off-time intervals in pulse-current electrodeposition. The gold film prepared under the optimum conditions showed an average grain size at 10.4 nm, and the compressive yield strength reached 800 MPa for a pillar-type micro-specimen having dimensions of 10 μm × 10 μm × 20 μm fabricated from the pulse-electrodeposited gold film. Average grain size of the pulse-electrodeposited gold film was much smaller, and the compressive yield strength was much higher than the values reported in other studies. The high strength is due to the grain boundary strengthening mechanism known as the Hall-Petch relationship. In general, the pulse-electrodeposited gold films showed yield strength ranging from 400 to 673 MPa when the average grain size varied by adjusting the pulse-electrodeposition parameters.

Keywords: pulse-current electrodeposition, gold material, micro-mechanical property, micro-compression test, Hall-Petch relationship

1. Introduction

Gold materials fabricated by electrodeposition are commonly used as contact materials in printed circuit boards, electrical connectors, relays, and micro- and nanoscale electronic components for many decades because of the high electrical conductivity, chemical stability, corrosion resistance, and ductility [1–5]. In recent years, gold has become a promising material as movable structures and proof masses in micro–electrical-mechanical system (MEMS) accelerometer devices, because of the high density (19.3×10^3 kg/m^3 at 298 K), which is about ten times higher than that of silicon (2.33×10^3 kg/m^3 at 298 K) [6]. However, gold is known to be a soft metallic material. The mechanical strength becomes a concern in further miniaturization of the MEMS device. The yield strength of bulk gold is reported to be 55–200 MPa [7], and the strength can be increased to 550 MPa when using specimens having sub-micro-dimensions because of the size effect [8]. Decreasing

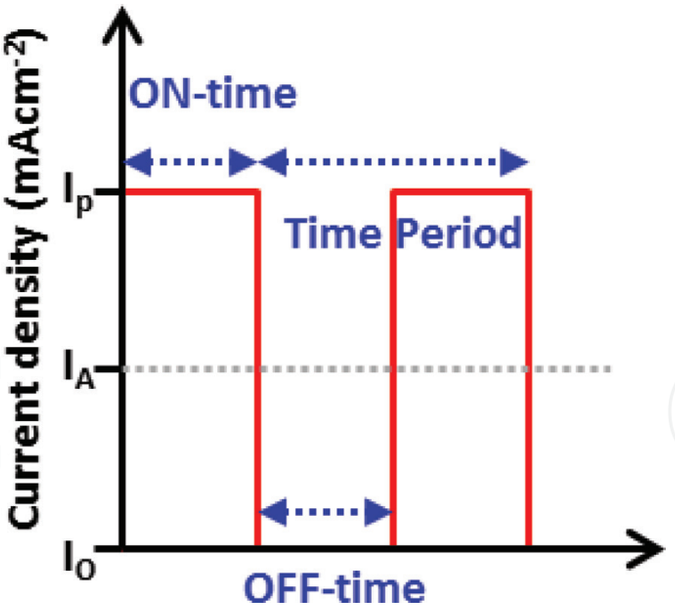

Figure 1.
Illustration of typical pulse-current waveform.

grain size of the gold materials is expected to allow further enhancement of the mechanical properties according to the Hall-Petch relationship [9, 10].

Pulse-current electrodeposition (PCE) has been reported to be effective in fabrication of gold materials with finer grains, higher uniformity, and lower porosity [11, 12] when compared with constant-current electrodeposition (CCE). Also, it is possible to control the microstructure and the film thickness by regulating the pulse-current amplitude (on-time current density and off-time current density) and the width (on-time and off-time interval), as shown in **Figure 1**. Most importantly, an increase in the nuclei density could be achieved to deposit films with finer grains. On the other hand, for evaluating mechanical properties of the deposited films, Vickers microhardness test is the most popular method. However, the hardness characteristics are often affected by the substrate. Vickers microhardness test cannot show the real strength of deposited films, especially for films having thickness in micro-/nanoscale. Therefore, it is necessary to characterize mechanical strength of the electrodeposited gold film by micro-mechanical testing method for practical applications in miniaturized devices.

In this chapter, gold films prepared by the PCE with a sulfite-based electrolyte showed less defect, lower surface roughness, finer grain size, and denser texture when compared with gold films prepared by the conventional CCE. Micro-mechanical properties of gold micro-specimens fabricated from the gold films prepared by the PCE and CCE were evaluated by micro-compression tests. To the best of our knowledge, this is the first report on micro-mechanical characterization of pure gold materials fabricated by PCE. Also, the electrodeposited pure gold film prepared by the PCE showed an ultrahigh strength of 800 MPa, which is the highest value reported for pure gold when compared with values reported in the literature.

2. Electrodeposition of gold

The gold electrolyte used in this study was a commercially available sulfite-based electrolyte provided by Matex Japan. The electrolyte contained 10 g/L of gold with pH of 8.0 and 5% sodium gluconate as the additive. Cu plates and Pt plates were used as the cathode and anode, respectively. For the PCE, the on-time current density (I_{on}) was 10 mA/cm^2, and the off-time current density (I_{off}) was 0 mA/cm^2.

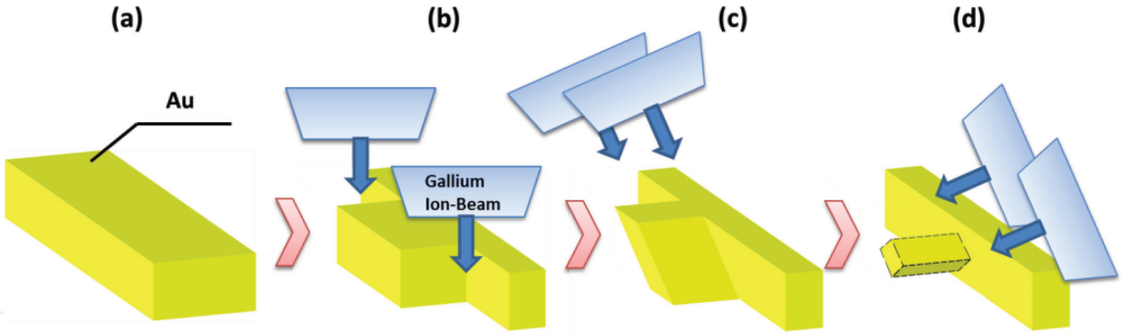

Figure 2.
Schematic images showing flow of the pillar-type micro-specimen fabrication steps. (a) Polished electrodeposited gold. (b) Size reduction of the specimen. (c) and (d) Finishing with a low intensity beam at a tilt angle of 45±1.7°.

The on-time interval (T_{on}) and the off-time interval (T_{off}) varied from 1 to 10 ms to study the effect on properties of the deposited gold film. The reaction temperature was 60°C for both PCE and CCE. For the CCE, the current density was fixed at 5 mA/cm^2, which is the same as the average current density of the PCE. A gold film was electrodeposited using a cyanide-based electrolyte containing 20 g/L of gold with pH of 5.0 to be used as the comparison reference specimen. The gold film was electrodeposited on a Pt substrate. The current density was 4 mA/cm^2, and the temperature was 60°C.

Morphology of the gold films was examined by an atomic force microscope (AFM, XE-100, Park System). The crystallographic structures of the films were investigated by an X-ray diffractometer (XRD, Ultima IV, Rigaku) at a glancing angle of 1.0°. The X-ray was generated by a Cu target operated at 40 kV and 40 mA. Average grain size was calculated using the Scherrer equation.

After the electrodeposition step, pillar-type micro-specimens were fabricated from the gold films by focused ion beam (FIB, FB2100, Hitachi) milling. Details of the fabrication process are shown in **Figure 2**. In order to minimize the tapering effect often observed in the FIB milling, instead of the conventional top-down milling process using irradiation along the pillar axis, the ion beam was irradiated from one side of the pillar at a tilt angle of 45 ± 1.7° as shown in **Figure 2(c)** and **(d)**. Therefore, the tapering effect can be minimized.

Dimensions of the fabricated micro-specimens had a square cross section with 10 μm in each side and a height of 20 μm. The compression tests were carried out using a test machine modified from a micro-indentation machine, which was specially designed for the micro-sized specimens and the compression test. The test machine was equipped with a flat-end diamond indenter and a piezoelectric actuator to control the displacement speed at 0.1 μm/s. The load resolution was 10 μN. Observation of the micro-specimens before and after the compression test was conducted using a scanning ion microscope (SIM) equipped within the FIB.

3. Pulse-current electrodeposition of ultrafine nanocrystalline gold

3.1 Properties of the electrodeposited gold film

Figure 3 shows the AFM micrographs of the gold films. The gold film electrodeposited with the cyanide-based electrolyte had hill-like bump morphology and a rough surface as shown in **Figure3(a)**. The surface roughness (R_a) was 117.1 nm. The gold film prepared by the CCE with the sulfite-based electrolyte showed irregular small dome-shaped bumps having a height of ca. 0.2–0.25 μm as shown in **Figure 3(b)**. On

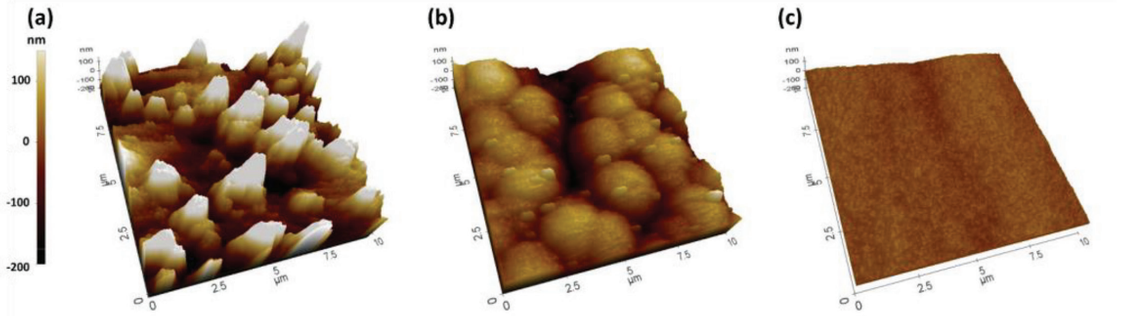

Figure 3.
AFM micrographs of (a) the gold film surface prepared by the CCE with the cyanide-based electrolyte, (b) the gold film surface prepared by the CCE, and (c) the PCE with the sulfite-based electrolyte.

the other hand, the gold film fabricated by the PCE with the sulfite-based electrolyte had a smooth and defect-free surface as shown in **Figure 3(c)**. For the CCE with the sulfite-based electrolyte, the surface roughness was 32.5 nm, whereas it was only 10.7 nm for the PCE with the sulfite-based electrolyte. The smooth surface achieved by the PCE is attributed to the enhanced desorption of the hydrogen gas bubbles during the off-time interval of the PCE, because the defects are suggested to be mainly caused by the hydrogen gas bubbles formed along with reduction of the gold ions.

Figure 4 shows XRD patterns of the gold films. All XRD patterns exhibited four peaks corresponding to the (111), (200), (220), and (311) planes of metallic face-centered cubic (FCC) gold (JCPDS No. 04-0784). The XRD results were similar to

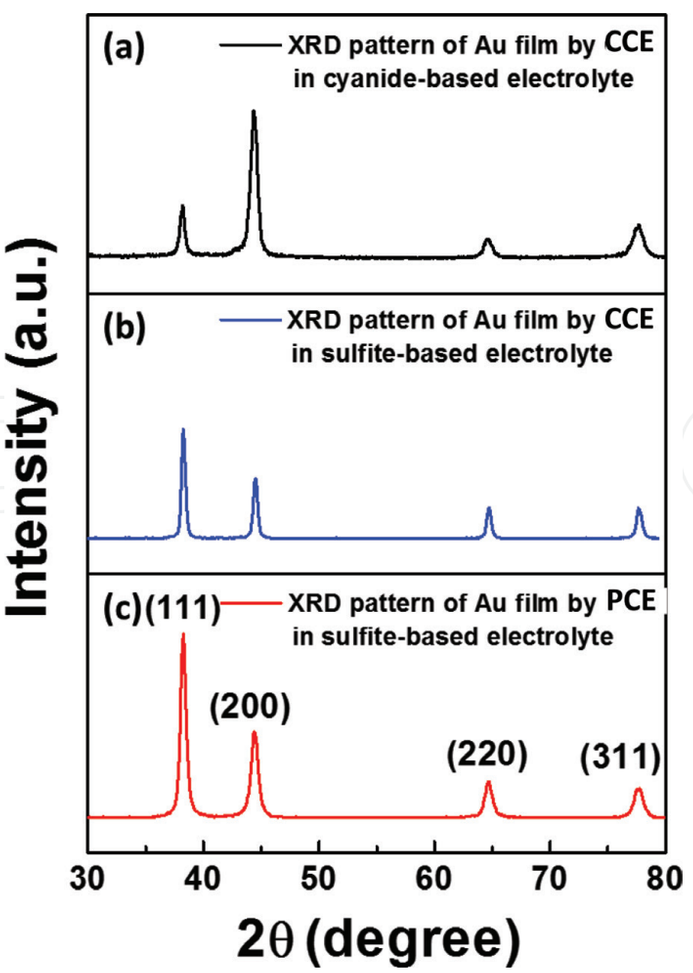

Figure 4.
X-ray diffraction patterns of (a) the gold film prepared by the CCE with the cyanide-based electrolyte, (b) the gold film prepared by the CCE, and (c) the PCE with the sulfite-based electrolyte.

the work reported by Bozzini et al. [13]. Unlike the reference gold film prepared with the cyanide-based electrolyte, the gold films fabricated with the sulfite-based electrolyte showed intense (111) orientation. It was reported that the surface energy of the (111) crystal growth orientation is the lowest when compared with the other crystal orientation for FCC metals, such as the (100) and the (110) planes [14]. Moreover, XRD peaks of gold films prepared by the PCE with the sulfite-based electrolyte were broader than those by the CCE. The estimated grain size of the gold film prepared by the PCE was 10.5 nm, which was much smaller than the grain size of 22.8 and 17.6 for the CCE with the sulfite-based electrolyte and the cyanide-based electrolyte, respectively. The grain refinement effect is attributed to the high on-time current density, which results in high nucleation rate during the on-time interval.

In summary, the AFM micrographs and XRD patterns indicate that smooth and defect-free gold film with ultrafine grain size of 10.5 nm can be achieved by the optimized parameters of the PCE. The grain size is smaller than the values reported in previous studies [15–17]. For the optimized PCE parameters, the pulse current is 10 mA/cm^2 and the off-time current is 0 mA/cm^2. On-time and off-time of the PCE are both 10 ms.

3.2 Mechanical properties of the gold micro-specimen

Microstructure of the micro-specimens before and after the compression test and the deformation behaviors was observed from the SIM images shown in **Figure 5**.

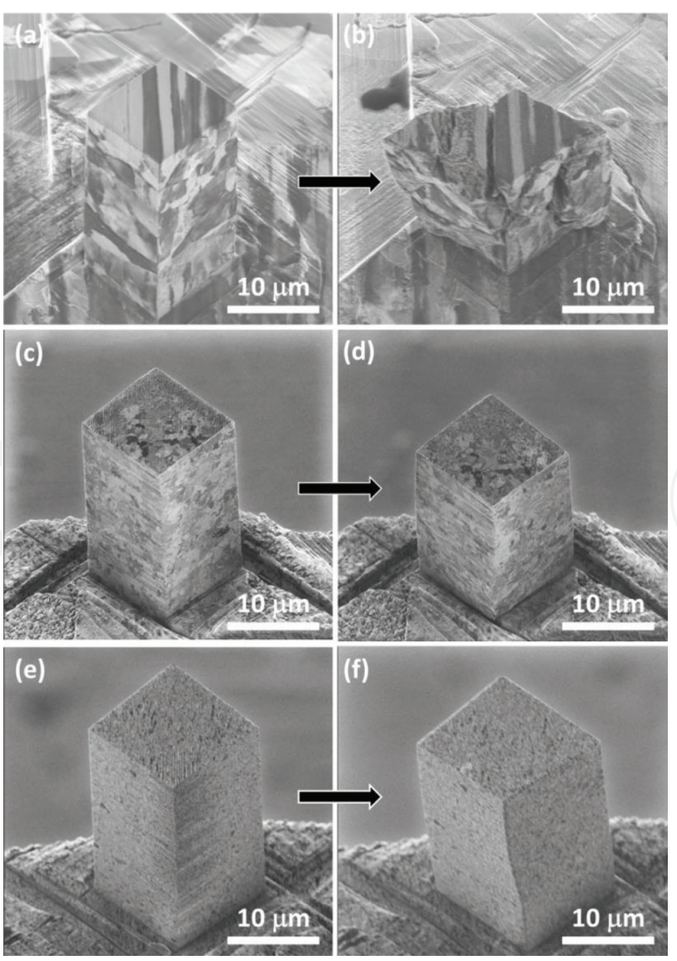

Figure 5.
SIM images of the (a) as-fabricated and (b) deformed gold micro-specimens fabricated from the CCE with the cyanide-based electrolyte, (c) the as-fabricated and (d) deformed gold micro-specimens fabricated from the CCE with the sulfite-based electrolyte, and the (e) as-fabricated and (f) deformed gold micro-specimens fabricated from the PCE with the sulfite-based electrolyte.

The ion channeling contrast shown in the SIM images indicates orientation changes of the textures on the sample surface. A gold micro-specimen was fabricated from the cyanide-based electrolyte to act as a comparison, and the results are shown in **Figure 5(a)** and **(b)**. White and gray irregular strip patterns in several μm orders were observed on both the top and sidewall surfaces, and these patterns are attributed to the columnar textures having a direction of perpendicular to the substrate/electrolyte interface. Cracks shown in **Figure 5(b)** indicate brittle fractures along the texture boundary, which suggest the brittle nature of the texture boundary. The grain size obtained from XRD was 17.6 nm, which is far smaller than the size of the patterns observed in the SIM image. While the contrast of the SIM image represents the crystal orientation against the beam direction, the boundaries observed in **Figure 5(a)** and **(b)** should be texture boundaries instead of grain boundaries. Camouflage pattern of the grain/structure was observed on surfaces of the gold micro-specimen prepared from the sulfite-based electrolyte, as shown in the SIM image in **Figure 5(c)**. The gold micro-specimen exhibited broad shear crossing from the top front to the bottom after ca. 10% of deformation, as shown in **Figure 5(d)**, which is similar to the deformation of electrodeposited nanocrystalline Ni [18]. In **Figure 5(e)**, there is no obvious grain/texture boundary on the surface of the gold micro-specimen, which is consistent with the XRD results that fine grains of 10.5 nm were results of the PCE since the SIM could not identify boundaries finer than ca. 1 μm. The ductile deformation shown in **Figure 5(f)** was attributed to the intrinsic property of ultrafine or nanocrystalline materials during the compressive deformation [19]. Although the grain size was different between the gold micro-specimens fabricated from gold films by the CCE and PCE with the sulfite-based electrolyte, the deformation behaviors were similar as shown in **Figure 5(d)** and **(f)**.

Figure 6(a) shows compressive engineering stress-strain curves generated from compression tests of the gold micro-specimens. Deformation behaviors of the micro-specimens prepared from the cyanide-based electrolyte were different from the micro-specimens prepared from the CCE and the PCE with the sulfite-based electrolyte. Yield drops observed in the stress-strain curve generated from compression test of the micro-specimen prepared from the cyanide-based electrolyte may correspond to the cracks observed in **Figure 5(b)**. The cracks are suggested to be caused by the impurities derived from the cyanide-based bath, which lead to a decrease in the adhesion between the textures. The micro-specimens prepared from the sulfite-based electrolyte by the CCE and PCE both showed parabolic hardening generally observed in polycrystalline samples. Notable work hardening observed in the micro-specimen prepared from the PCE with the sulfite-based electrolyte could be a consequence of the reduction in defects by the PCE. A summary of the strengths obtained from this work and from the literatures is shown in **Figure 6(b)**. The strengths obtained in this work followed the Hall-Petch relationships well and reached 800 MPa. To the best of our knowledge, a compressive strength of 800 MPa is the highest value reported for electrodeposited pure gold [7, 8, 20, 21]. Also, the gold film prepared by the PCE showed large work hardening which indicates high ductility and malleability of the material.

3.3 Effects of the on-time and off-time intervals

The T_{on} and T_{off} varied from 1 to 10 ms to study the effect on the microstructure. Detailed information of the PCE parameters is given in **Figure 7**. SIM images of the three micro-specimens fabricated from the gold films pulse electrodeposited with three different on- and off-time combinations are shown in **Figure 8**. **Figure 8(d)**–**(f)** shows a side view of the micro-specimens A, B, and C, respectively. The contrast observed in the SIM images represents the grain/texture boundaries. Two types of

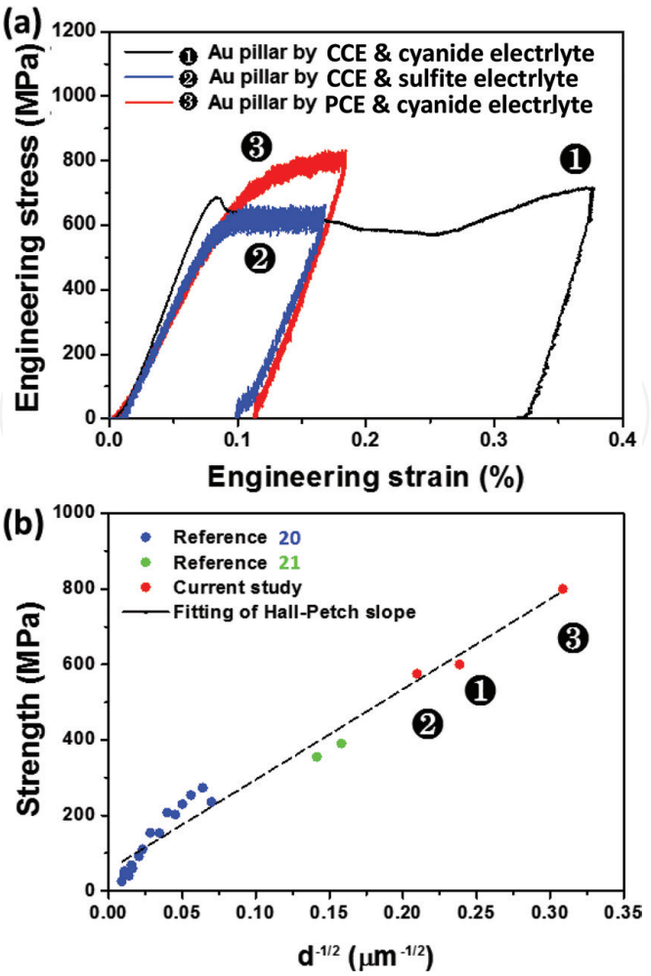

Figure 6.
Engineering stress-strain curves obtained from the micro-compression test of the gold micro-specimens and (b) Hall-Petch plot of polycrystalline gold micro-specimens.

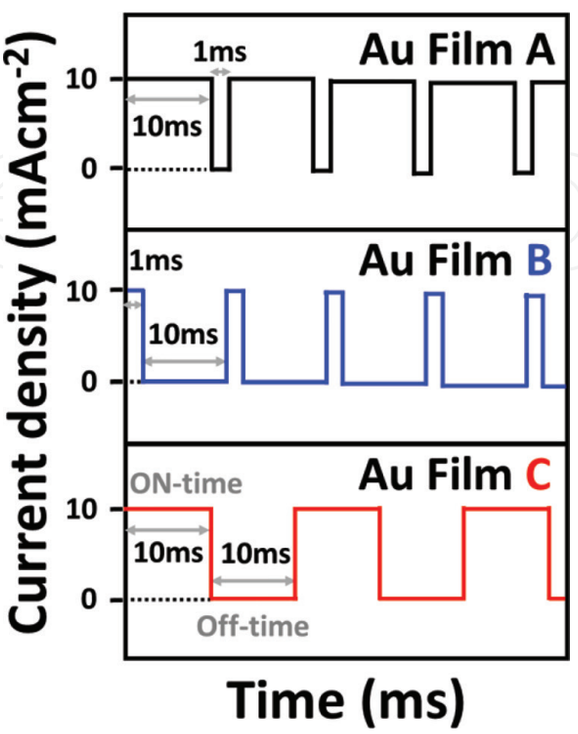

Figure 7.
Parameters of pulse-current waveform used in the PCE-fabricated gold films A, B, and C.

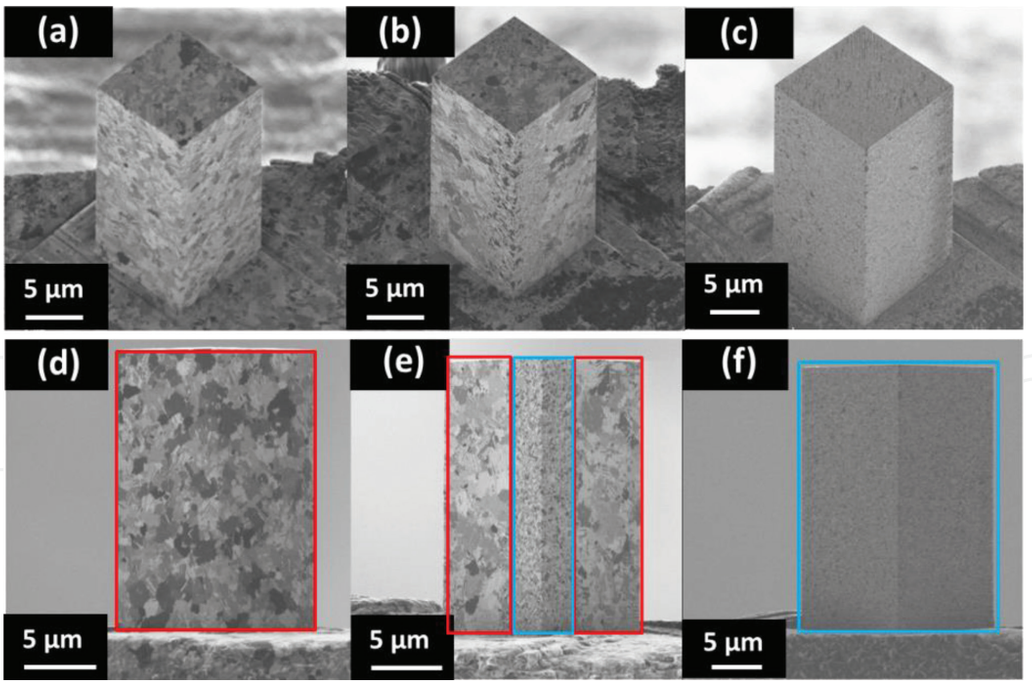

Figure 8.
SIM images of the as-fabricated micro-specimens A (a), B (b), and C (c) and side views of the as-fabricated micro-specimens A (d), B (e), and C (f). In the area surrounded by red full line, grains of several hundred nanometers (shown as red-dotted line) and heterogeneous pattern were observed. In the area surrounded by red full line, no obvious grain/texture boundary was observed.

grain structures were observed between **Figure 8(d)** and **(f)**. For micro-specimen A (**Figure 8(a)** and **(d)**), most of the grains were in micrometer order. Only a few grains having sizes less than 1 μm were observed. One of the relatively large grains is clearly shown in the enlarged image surrounded by red-dotted line in **Figure 8(d)**. The grain structure of micro-specimen A was considered to be composed of non-homogeneous mixture of micro-grains and nano-grains. For the second type shown in micro-specimen C (**Figure 8(c)** and **(f)**), there were no obvious grain/texture boundaries observed from the SIM image. The film was considered to be composed of homogeneous nano-grains, in which details of the boundaries were beyond the detection limit of the SIM. Micro-specimen B (**Figure 8(b)** and **(e)**) showed a mixture of the two grain structure types. The nano-grains similar to those in micro-specimen C were located in the front corner as shown in **Figure 8(b)**.

It could be concluded that intervals of 10 ms for both the T_{on} and T_{off} were the optimized conditions to achieve uniform nano-grains; in such PCE conditions, the grain nucleation dominated in the gold reduction reaction rather than grain growth of the already-existing grains. During the T_{off} interval, the depleted surface concentration of gold ions on the cathode can be replenished by the diffusion of gold ions from the bulk electrolyte, and as-formed by-products during the reaction would diffuse away from the cathode surface. New nuclei are more likely to form because of the high-surface concentration of gold ions during the T_{on} interval. In the case of micro-specimen A, the T_{off} of 1 ms was too short, and it was insufficient for the gold ion replenishment. The low-surface gold ion concentration led to the large grain growth. Also, the short T_{off} promoted continuous growth of the already-existing grains. Therefore, the electrodeposition condition became similar to the CCE, which leads to similar grain structures with the CCE. The results suggest that the T_{on} should be short enough to confirm the gold ion consumed in each T_{on} period, which could be sufficiently replenished during the T_{off} period. When the T_{on} is too long, the electrodeposition condition would be close to the CCE conditions and leads to large grains and occurrence of side reactions. On the other hand, T_{on} cannot be too

short. It should be long enough to allow full charge of the electrical double layer. Otherwise, the reduction reaction cannot be initiated properly. For micro-specimen B, T_{on} of 1 ms may be too short to fully charge the double layer. Moreover, Molina et al. reported that the calculated critical radius of the nuclei of nickel film became much larger, when T_{on} of 1 ms was applied. Also, the nucleation rate is much lower when too short T_{on} was used [22]. The result of micro-specimen B was in agreement with results reported by Molina et al., in which the short T_{on} of 1 ms used in micro-specimen B led to the large grain growth due to the low nucleation rate and large critical size of nuclei.

SEM images of micro-specimens A, B, and C before and after the compression test are shown in **Figure 9**. All the gold micro-specimens showed broad shear crossing from top to bottom of the micro-specimens, and protrusions on sidewalls of the micro-specimen were observed after the deformation. Formation of the protrusions was attributed to the grain boundary slip occurred during the compression test, because the micro-specimens in this study were composed of polycrystals.

Yield strengths of the micro-specimens were determined from the engineering stress-strain curves given in **Figure 10**. By assuming volume conservation during the plastic deformation, the engineering stress σ is defined in the following equation:

$$\sigma = P/S \tag{1}$$

where P is the measured force and S is the cross-sectional area. The engineering strain ε can be calculated as the following equation:

$$\varepsilon = \Delta L/L_0 \tag{2}$$

where ΔL is the applied displacement and L_0 is the initial length of the micro-specimen. Both of the P and the ΔL were acquired by the test machine. The S and the L_0 were both obtained from SEM observations. The flow stresses of micro-specimen A and micro-specimen B were 440 and 600 MPa, respectively. Micro-specimen C showed the highest flow stress of 800 MPa. These differences of flow

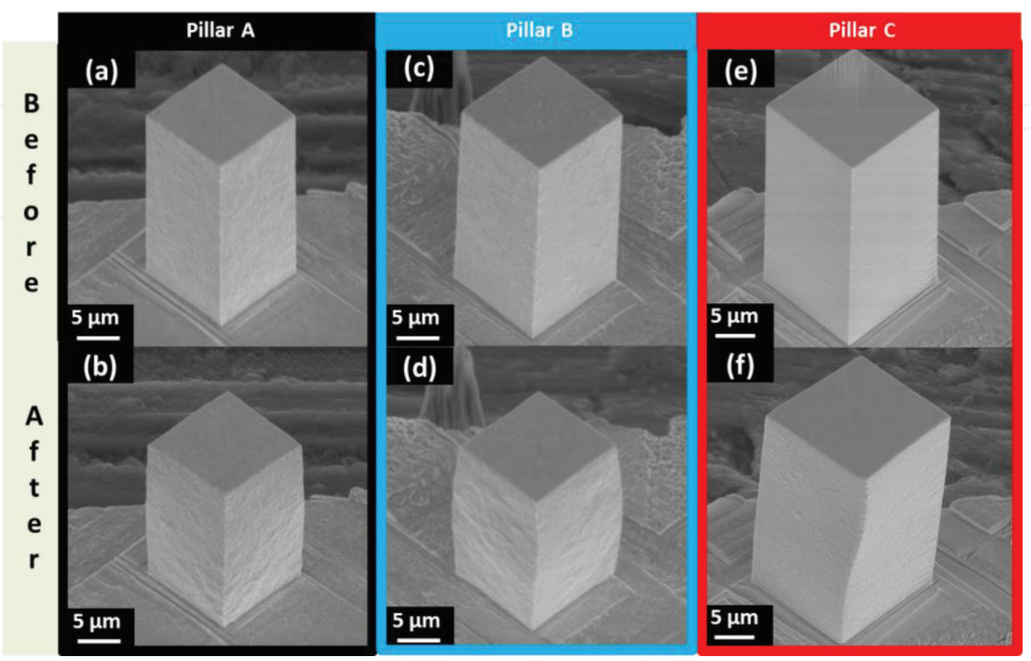

Figure 9.
SEM images of the (a) as-fabricated and (b) deformed micro-specimen A, the (c) as-fabricated and (d) deformed micro-specimen B, and the (e) as-fabricated and (f) deformed micro-specimen C.

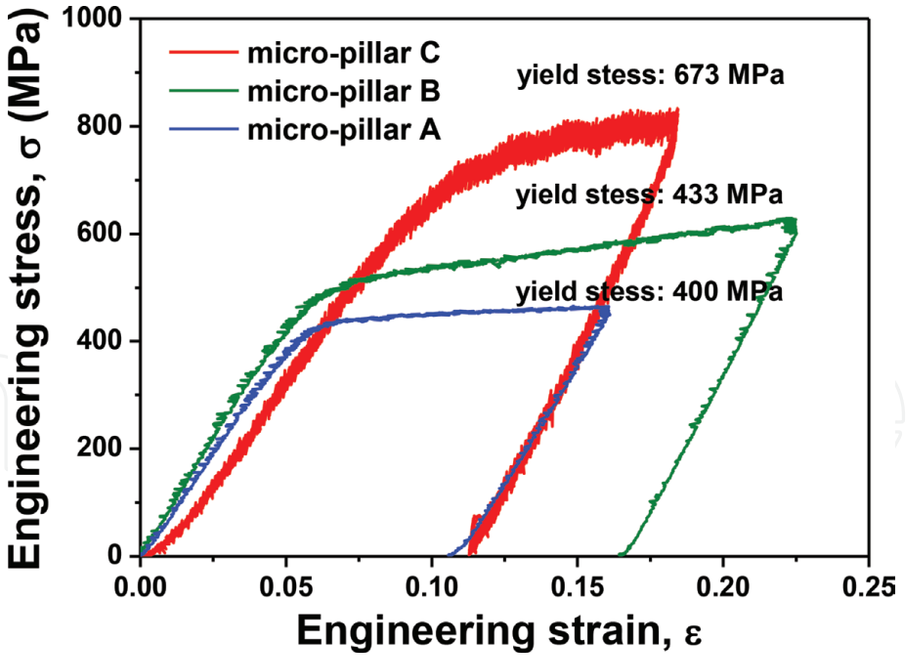

Figure 10.
Engineering stress-strain curves obtained from the micro-compression tests of the gold micro-specimens.

stress are due to structural differences, i.e., grain size. As the grain size becomes smaller, the strength becomes higher due to the grain boundary strengthening mechanism or well expressed as the Hall-Petch effect [20]. Hall and Petch had concluded that the yield strength can be expressed as.

$$\sigma = \sigma_0 + k_y d^{-1/2} \tag{3}$$

where σ is the yield strength, σ_o is a material constant for the starting stress for dislocation movement (or the resistance of the lattice to dislocation motion), k_y is the strengthening coefficient (a constant specific to each material), and d is the average grain diameter. To confirm if the Hall-Petch relationship holds in this work, we measured yield strength and grain size of the films. **Figure 9** shows the yield strength measured at a plastic strain of 0.2%. For micro-specimens A, B, and C, the yield strengths were 400, 433, and 673 MPa (compressive strength of 800 MPa), respectively. Although the yield strength was only slightly higher for micro-specimen A when compared with micro-specimen B, the enhanced work hardening demonstrates the effect of the partially nano-grained region in micro-specimen B. In addition, SEM observation shown in **Figure 8(d)** shows smooth deformation morphology at the front corner of micro-specimen B, which indicates a resistance to the deformation by the nano-grained region. The fully nano-grained micro-specimen C had a yield strength of 673 MPa, which is the highest value for pure gold reported when compared with the literature within our reach [7, 20, 23]. XRD diffraction patterns and the Scherrer equation were used to estimate the grain size of the film C. The Scherrer equation was given in the following equation:

$$g = \frac{\lambda}{\beta \cos\theta} \tag{4}$$

where g, λ, β, and θ are the average grain size, X-ray wavelength (0.15418 nm), full width at half maximum in radians, and Bragg angle, respectively. The estimated grain size was 10.4 nm. The nano-scale grain size agrees well with the outstandingly high strength observed in this work.

In summary, it can be deduced that the T_{on} of 10 ms and T_{off} of 10 ms are the optimum parameters for the PCE of gold with a sulfite-based electrolyte, because the grain size reached ca. 10 nm and the compressive strength of 800 MPa (yield strength of 673 MPa) was much higher than the other micro-specimens evaluated in this study. These results demonstrate that the PCE is promising for MEMS applications since it demonstrates a simple method to control the grain size and the mechanical strength of gold micro-components by regulating the PCE T_{on} and T_{off} intervals.

4. Conclusion

Pulse-current electrodeposition and a non-cyanide sulfite-based electrolyte were used in fabrication of gold films toward fabrication of MEMS components. The pulse-current electrodeposition with different combinations of the T_{on} and T_{off} were investigated to evaluate the influence on the film properties and the micro-mechanical properties. Surface of the PCE gold films possessed less defect, lower roughness, smaller grain size, and denser texture than the gold film prepared by the constant-current electrodeposition. Micro-mechanical properties of the pulse-current plated gold films were evaluated by micro-compression tests using pillar-type micro-specimens fabricated from the gold films by FIB milling. For both the T_{on} and the T_{off}, 10 ms was concluded to be the optimum condition to achieve uniform nano-grained films. The finest grain size reached 10.4 nm for the PCE gold film. The compressive strength was 800 MPa (yield strength of 673 MPa) for the specimen having dimensions of 10 μm × 10 μm × 20 μm fabricated from the PCE gold film. For the deformation behavior, all the micro-specimens showed promoted surface relief phenomenon after the compression tests. All of the gold micro-specimens had a yield strength higher than 400 MPa, which was much higher than that of the bulk gold. The grain size was much smaller, and the compressive strength obtained was much higher than the values reported in other studies. The high strength is suggested to be due to the grain boundary strengthening mechanism known as the Hall-Petch effect. The results demonstrate that the PCE method with the sulfite-based electrolyte is effective to control the microstructure and enhance the mechanical strength of gold materials for applications in miniaturized electronic devices.

Acknowledgements

This work was supported by JST CREST Grant Number JPMJCR1433 and by the Grants-in-Aid for Scientific Research (S) (JSPS KAKENHI Grant Number 26220907).

Conflict of interest

We have no conflict of interest to declare.

Author details

Chun-Yi Chen[1*], Masaharu Yoshiba[1], Haochun Tang[1], Tso-Fu Mark Chang[1], Takashi Nagoshi[2], Daisuke Yamane[1], Toshifumi Konishi[3] and Katsuyuki Machida[1]

1 Institute of Innovative Research, Tokyo Institute of Technology, Yokohama, Japan

2 National Institute of Advanced Industrial Science and Technology (AIST), Ibaraki, Japan

3 NTT Advanced Technology Corporation, Atsugi, Kanagawa, Japan

*Address all correspondence to: chen.c.ac@m.titech.ac.jp

IntechOpen

References

[1] Togasaki N, Okinaka Y, Homma T, Osaka T. Preparation and characterization of electroplated amorphous gold-nickel alloy from electrical contact applications. Electrochimica Acta. 2005;**51**:882-887. DOI: 10.1016/j.electacta.2005.04.057

[2] Kato M, Senda K, Musha Y, Sasano J, Okinaka Y, Osaka T. Electrodeposition of amorphous gold alloy films. Electrochimica Acta. 2007;**53**:11-15. DOI: 10.1016/j.electacta.2007.01.045

[3] Yamachika N, Musha Y, Sasano J, Senda K, Kato M, Okinaka Y, et al. Electrodeposition of amorphous au-Ni alloy film. Electrochimica Acta. 2008;**53**:4520-4527. DOI: 10.1016/j.electacta.2008.01.018

[4] Brun E, Durut F, Botrel R, Theobald M, Legaie O, Popa I, et al. Influence of the electrochemical parameters on the properties of electroplated Au-Cu alloys. Journal of the Electrochemical Society. 2011;**158**:D223-D227. DOI: 10.1149/1.3554727

[5] Homma H. Plating technology for electronics packaging. Electrochimica Acta. 2001;**47**:75-84. DOI: 10.1016/S0013-4686(01)00591-6

[6] Yamane D, Konishi T, Matsushima T, Machida K, Toshiyoshi H, Masu K. Design of sub-1g microelectromechanical systems accelerometers. Applied Physics Letters. 2014;**104**:074102-1-074102-4. DOI: 10.1063/1.4865377

[7] Greer JR, Oliver WC, Nix WD. Size dependence of mechanical properties of gold at the micron scale in the absence of strain gradients. Acta Materialia. 2005;**53**:1821-1830. DOI: 10.1016/j.actamat.2004.12.031

[8] Espinosa HD, Prorok BC, Peng B. Plasticity size effects in free-standing submicron polycrystalline FCC films subjected to pure tension. Journal of the Mechanics and Physics of Solids. 2004;**52**:667-689. DOI: 10.1016/j.jmps.2003.07.001

[9] Hall EO. The deformation and ageing of mild steel: II characteristics of the Lüders deformation. Proceedings of the Physical Society. Section B. 1951;**64**:747-753

[10] Petch NJ. The cleavage strength of polycrystals. Journal of the Iron and Steel Institute. 1953;**174**:25-28

[11] Horkens J, Romankiw LT. Pulsed potentiostatic deposition of gold from solutions of the Au (I) sulfite complex. Journal of the Electrochemical Society. 1977;**124**:1499-1505

[12] Ruffoni A, Landolt D. Pulse-plating of Au-Cu-Cd alloys: II. Theoretical modelling of alloy composition. Electrochimica Acta. 1988;**33**:1281-1289. DOI: 10.1016/0013-4686(88)80116-6

[13] Bozzini B, Fanigliulo A, Serra M. Electrodeposition of star-shaped gold crystallites. Journal of Crystal Growth. 2001;**231**:589-598. DOI: 10.1016/S0022-0248(01)01513-5

[14] Udler D, Seidman DN. Grain boundary and surface energies of fcc metals. Physical Review B. 1996;**54**:R11133-R11136

[15] Lee Y, Ahn SK, Roh Y. Comparison of nanometer-scale gold structures electrodeposited on Au and Pt seed electrode. Surface and Coating Technology. 1995;**193**:137-141. DOI: 10.1016/j.surfcoat.2004.07.055

[16] Chandrasekar MS, Pushpavanam M. Pulse and pulse reverse plating

conceptual, advantages and applications. Electrochimica Acta. 2008;**53**:3313-3322. DOI: 10.1016/j.electacta.2007.11.054

[17] Yevtushenko O, Natter H, Hempelmann R. Grain-growth kinetics of nanostructured gold. Thin Solid Films. 2006;**515**:353-356. DOI: 10.1016/j.tsf.2005.12.098

[18] Nagoshi T, Mutoh M, Chang T-FM, Sato T, Sone M. Sample size effect of electrodeposited nickel with sub-10 nm grain size. Materials Letters. 2014;**117**:256-259. DOI: 10.1016/j.matlet.2013.12.017

[19] Jia D, Ramesh KT, Ma E. Effects of nanocrystalline and ultrafine grain sizes on constitutive behavior and shear bands in iron. Acta Materialia. 2003;**51**:3495-3509. DOI: 10.1016/S1359-6454(03)00169-1

[20] Gan Z, He Y, Liu D, Zhang B, Shen L. Hall–Petch effect and strain gradient effect in the torsion of thin gold wires. Scripta Materialia. 2014;**87**:41-44. DOI: 10.1016/j.scriptamat.2014.05.011

[21] Emery RD, Povirk GL. Tensile behavior of free-standing gold films. Part II. Fine-grained films. Acta Materialia. 2003;**51**:2079-2087. DOI: 10.1016/S1359-6454(03)00007-7

[22] Molina J, Hoyos BA. Modeling of grain size and hardness for pulse current electroplating. Electrochimica Acta. 2009;**54**:1784-1790. DOI: 10.1016/j.electacta.2008.10.002

[23] Emery RD, Povirk GL. Tensile behavior of free-standing gold films. Part I. Coarse-grained films. Acta Materialia. 2003;**51**:2067-2079. DOI: 10.1016/S1359-6454(03)00006-5